

**A Finite Element-Boundary Integral Method for Scattering
and Radiation by Two- and Three-Dimensional Structures**

Authors: Jian-Ming Jin, John L. Volakis and Jeffery D. Collins

March 1991

National Aeronautics and
Space Administration
Ames Research Center
Moffett Field, CA 94035
Grant NAG-2-541

(NASA-CR-188071) A FINITE ELEMENT-BOUNDARY
INTEGRAL METHOD FOR SCATTERING AND RADIATION
BY TWO- AND THREE-DIMENSIONAL STRUCTURES
(Michigan Univ.) 39 p

CSCL 20N

N91-20359

Unclass
0005407

G3/32



THE UNIVERSITY OF MICHIGAN

Radiation Laboratory

**Department of Electrical Engineering
and Computer Science**

Ann Arbor, Michigan 48109-2122

USA

TECHNICAL REPORT

FOR

NASA Grant NAG-2-541

NASA Technical Monitor: Alex Woo

Grant Title: A NEW TECHNIQUE FOR SIMULATING
COMPOSITE MATERIAL

Report Title A Finite Element - Boundary Integral Method for Scattering
and Radiation by Two- and Three-Dimensional Structures

Institution: The Radiation Laboratory
Department of Electrical Engineering
and Computer Science
The University of Michigan
Ann Arbor, MI 48109-2122

Period Covered: March 1991

Report Authors Jian-Ming Jin and Jeffrey Collins

Principal Investigator: John L. Volakis
Telephone: (313) 764-0500

A FINITE ELEMENT – BOUNDARY INTEGRAL METHOD FOR
SCATTERING AND RADIATION BY TWO- AND
THREE-DIMENSIONAL STRUCTURES

Jian-Ming Jin, John L. Volakis, and Jeffery D. Collins

Radiation Laboratory

Department of Electrical Engineering and Computer Science

The University of Michigan

Ann Arbor, Michigan 48109-2122

ABSTRACT

This paper presents a review of a hybrid finite element – boundary integral formulation for scattering and radiation by two- and three-dimensional composite structures. In contrast to other hybrid techniques involving the finite element method, the proposed one is in principle exact and can be implemented using a low $O(N)$ storage. This is of particular importance for large scale applications and is a characteristic of the boundary chosen to terminate the finite element mesh, usually as close to the structure as possible. A certain class of these boundaries lead to convolutional boundary integrals which can be evaluated via the fast Fourier transform (FFT) without a need to generate a matrix, thus, retaining the $O(N)$ storage requirement. The paper begins with a general description of the method. A number of two- and three-dimensional applications are then given, including numerical computations which demonstrate the method's accuracy, efficiency and capability.

I. INTRODUCTION

Integral equation methods and to a lesser degree differential equation methods are commonly used for electromagnetic scattering and radiation computations. Among the various integral equation approaches, surface formulations (see, for example, [1]-[4]) are more attractive for perfectly conducting, impedance or layered material structures, whereas volume formulations (see, for example, [5]-[8]) are particularly suited for modeling inhomogeneous scatterers. Both have been applied to a variety of two- and three-dimensional problems and are often referred to as exact techniques because they guarantee convergence for sufficiently dense discretizations. However, they have the disadvantage of being difficult to implement for complex objects and also result in full matrices whose treatment requires a large memory. This is particularly true for three-dimensional applications and because of it, differential equation approaches are becoming more popular.

Differential equation methods can be subdivided into finite element and finite difference methods. In contrast to the integral equation approaches, they lead to relatively simple formulations and are thus attractive for simulating complex penetrable structures. More importantly, they are associated with sparse, banded matrices which can be efficiently solved and stored. They do not, however, incorporate the Sommerfeld radiation condition and this requires that the domain of discretization be extended far from the scatterer where the radiation condition can be imposed [9]. This is a major disadvantage of the differential equation methods and recent efforts have concentrated on the use of absorbing boundary conditions to reduce the discretization region outside the scatterer (see, for example, [10], [11]). Unfortunately, the accuracy of the absorbing boundary

conditions is dependent upon the composition and shape of the scatterer, leading to results of unpredictable accuracy.

To eliminate the disadvantages of the integral and differential equation methods while retaining their advantages, various hybrid methodologies have been developed (see, for example, [12]-[17]). The general principle of hybrid techniques is to introduce a fictitious boundary enclosing the scatterer. Interior to the boundary, the finite element or finite difference method is used to formulate the fields whereas in the exterior region the fields are represented by an eigenfunction expansion [12]-[14] or a boundary integral [15]-[17]. The last is an exact representation, but in practice the eigenfunction expansion is approximate since the infinite series must be truncated.

In this paper, we describe a hybrid technique which combines the finite element and boundary integral methods. The paper is essentially a review of our recent work pertaining to the development of a finite element – boundary integral method [18]-[24]. In the next section we present the general formulation without reference to any specific geometry or application. A number of two- and three-dimensional applications are then considered to demonstrate the accuracy, efficiency and capability of the method. Of particular concern in these applications is the choice of the fictitious boundary enclosing the structure so that the resulting boundary integrals are convolutions. They can then be evaluated via the fast Fourier transform (FFT) in conjunction with an iterative solution approach such as the conjugate gradient (CG) or biconjugate gradient (BiCG) method. In this manner, the generation of a partly full matrix is avoided and the solution requires only $O(N)$ storage without compromise in accuracy. Also, provided the enclosure fits tightly over the structure, the elements comprising the mesh outside the domain of the

structure are kept to a minimum.

II. GENERAL FORMULATION

Consider the scattering/radiation problem illustrated in Figure 1. We are interested in the computation of the fields generated by the external sources (\mathbf{J}^{ext} , \mathbf{M}^{ext}) (for the scattering case) or by the internal sources (\mathbf{J}^{int} , \mathbf{M}^{int}) (for the radiation case) in the presence of a three-dimensional structure immersed in an infinite, homogeneous medium. In the following we describe a numerical procedure for determining the field everywhere by combining the finite element and boundary integral methods.

1. Decoupling and Coupling of Exterior and Interior Fields

To combine the finite element and boundary integral methods, it is necessary that the three-dimensional structure be enclosed in a fictitious surface denoted by S . Within S the finite element method is employed to formulate the fields, whereas outside S the fields are represented by the radiation of the external sources and a set of equivalent electric and magnetic currents placed on S . This permits the decoupling of the fields interior and exterior to S which can later be coupled by enforcing tangential field continuity on S leading to a system of equations for the solution of the equivalent electric and magnetic currents.

By making use of the free space Green's function, the fields in the region exterior to S (this region will be hereon denoted as V_∞) are represented as

$$\mathbf{E} \text{ (or } \mathbf{H}) = \mathbf{E}^{inc} \text{ (or } \mathbf{H}^{inc}) + \mathbf{L}_{e,h}^s (\mathbf{E}^+ \times \hat{\mathbf{n}}, \mathbf{H}^+ \times \hat{\mathbf{n}}) \quad (1)$$

where $(\mathbf{E}^{inc}, \mathbf{H}^{inc})$ denote the incident fields radiated by the impressed external sources

$(\mathbf{J}^{ext}, \mathbf{M}^{ext})$ and $\mathbf{L}_{e,h}^s$ denote the boundary/surface operators (integral or integro-differential) yielding the field radiated by the equivalent electric $(\mathbf{H}^+ \times \hat{\mathbf{n}})$ and magnetic $(\mathbf{E}^+ \times \hat{\mathbf{n}})$ currents. The subscript e corresponds to the operator associated with the E field formulation and likewise the subscript h is associated with the H field representation. Also, $(\mathbf{E}^+, \mathbf{H}^+)$ are the fields on S as one approaches from V_∞ and $\hat{\mathbf{n}}$ denotes the unit vector normal to S and pointing toward V_∞ . Let us now consider the region interior to S , denoted as V . When this region is inhomogeneous, its associated Green's function is usually not available and we cannot, therefore, formulate the fields in terms of boundary integrals as was done for V_∞ . However, by using the differential form of Maxwell's equations, we can find a relation between the interior and the tangential boundary fields. This can be of the form

$$f_{e,h}(\mathbf{E} \text{ or } \mathbf{H}, \mathbf{E}^- \times \hat{\mathbf{n}}, \mathbf{H}^- \times \hat{\mathbf{n}}) = 0 \quad (2)$$

where $f_{e,h}$ denote the appropriate operators and $(\mathbf{E}^-, \mathbf{H}^-)$ are the fields on S as one approaches from V . We note that, since $f_{e,h}$ do not involve any Green's function, their discretization via the finite element method results in sparse and banded matrices. Consequently, the implementation of (2) is associated with $O(N)$ memory demand which is one of the primary advantages of the finite element method.

To solve for $(\mathbf{E}^\pm \times \hat{\mathbf{n}}, \mathbf{H}^\pm \times \hat{\mathbf{n}})$ we must couple the fields given in (1) and (2) by enforcing continuity of the tangential electric and magnetic fields on S . The continuity condition demands that

$$\mathbf{E}^+ \times \hat{\mathbf{n}} = \mathbf{E}^- \times \hat{\mathbf{n}}, \quad \mathbf{H}^+ \times \hat{\mathbf{n}} = \mathbf{H}^- \times \hat{\mathbf{n}} \quad (3)$$

which together with (1) and (2) imply a system for the solution of the interior and

boundary fields.

2. Formulation of Functionals and Weighted Residual Equations

To formulate the fields in V , we begin with the vector wave equation

$$\nabla \times \left(\frac{1}{\mu_r} \nabla \times \mathbf{E} \right) - k_0^2 \epsilon_r \mathbf{E} = -jk_0 Z_0 \mathbf{J}^{int} + \nabla \times \left(\frac{1}{\mu_r} \mathbf{M}^{int} \right) \quad (4)$$

where $k_0 = 2\pi/\lambda$ is the free space wavenumber and Z_0 is the free space intrinsic impedance. A traditional approach for solving this is to consider the functional

$$\begin{aligned} F(\mathbf{E}) = & \frac{1}{2} \iiint_V \left[\frac{1}{\mu_r} (\nabla \times \mathbf{E}) \cdot (\nabla \times \mathbf{E}) - k_0^2 \epsilon_r \mathbf{E} \cdot \mathbf{E} \right] dV \\ & + \iiint_V \mathbf{E} \cdot \left[jk_0 Z_0 \mathbf{J}^{int} - \nabla \times \left(\frac{1}{\mu_r} \mathbf{M}^{int} \right) \right] dV \\ & + jk_0 Z_0 \oint_S \mathbf{E} \cdot (\mathbf{H} \times \hat{\mathbf{n}}) dS \end{aligned} \quad (5)$$

which can be easily shown to be stationary with respect to the solution of (4) with $(\mathbf{H} \times \hat{\mathbf{n}})$ being considered as one of the sources for \mathbf{E} . Thus \mathbf{E} can be found by enforcing

$$\delta F(\mathbf{E}) = 0 \quad (6)$$

where $\delta F(\mathbf{E})$ denotes the first order variation of F about \mathbf{E} .

An alternative approach for solving (4) is to employ the method of weighted residuals. This is an approach often presented in graduate electromagnetics texts and it would, therefore, be instructive to employ it here as well. Based on the weighted residual method we demand that

$$\begin{aligned} \langle \mathbf{R}, \mathbf{T} \rangle = & \iiint_V \left[\nabla \times \left(\frac{1}{\mu_r} \nabla \times \mathbf{E} \right) \cdot \mathbf{T} - k_0^2 \epsilon_r \mathbf{E} \cdot \mathbf{T} \right] dV \\ & + \iiint_V \mathbf{T} \cdot \left[jk_0 Z_0 \mathbf{J}^{int} - \nabla \times \left(\frac{1}{\mu_r} \mathbf{M}^{int} \right) \right] dV = 0 \end{aligned} \quad (7)$$

where \mathbf{R} denotes the residual of (4) and \mathbf{T} is a testing or weighting function chosen to satisfy the required boundary conditions associated with \mathbf{E} . Recalling the identity

$$\begin{aligned} & \iiint_V \nabla \times \left(\frac{1}{\mu_r} \nabla \times \mathbf{E} \right) \cdot \mathbf{T} \, dV \\ &= \iiint_V \frac{1}{\mu_r} (\nabla \times \mathbf{E}) \cdot (\nabla \times \mathbf{T}) \, dV + jk_0 Z_0 \oint_S \mathbf{T} \cdot (\mathbf{H} \times \hat{\mathbf{n}}) \, dS \end{aligned} \quad (8)$$

(7) can be written as

$$\begin{aligned} \langle \mathbf{R}, \mathbf{T} \rangle &= \iiint_V \left[\frac{1}{\mu_r} (\nabla \times \mathbf{E}) \cdot (\nabla \times \mathbf{T}) - k_0^2 \epsilon_r \mathbf{E} \cdot \mathbf{T} \right] \, dV \\ &+ \iiint_V \mathbf{T} \cdot \left[jk_0 Z_0 \mathbf{J}^{int} - \nabla \times \left(\frac{1}{\mu_r} \mathbf{M}^{int} \right) \right] \, dV \\ &+ jk_0 Z_0 \oint_S \mathbf{T} \cdot (\mathbf{H} \times \hat{\mathbf{n}}) \, dS = 0 \end{aligned} \quad (9)$$

which is equivalent to (5) and (6) provided \mathbf{T} is chosen to be the same as the expansion basis, implying an application of Galerkin's technique.

In some cases, it may be advantageous to work with magnetic fields rather than electric fields. It will then be necessary to use the dual of (5) and (9) given by

$$\begin{aligned} F(\mathbf{H}) &= \frac{1}{2} \iiint_V \left[\frac{1}{\epsilon_r} (\nabla \times \mathbf{H}) \cdot (\nabla \times \mathbf{H}) - k_0^2 \mu_r \mathbf{H} \cdot \mathbf{H} \right] \, dV \\ &- \iiint_V \mathbf{H} \cdot \left[jk_0 Y_0 \mathbf{M}^{int} + \nabla \times \left(\frac{1}{\epsilon_r} \mathbf{J}^{int} \right) \right] \, dV \\ &- jk_0 Y_0 \oint_S \mathbf{H} \cdot (\mathbf{E} \times \hat{\mathbf{n}}) \, dS \end{aligned} \quad (10)$$

and

$$\begin{aligned} \langle \mathbf{R}, \mathbf{T} \rangle &= \iiint_V \left[\frac{1}{\epsilon_r} (\nabla \times \mathbf{H}) \cdot (\nabla \times \mathbf{T}) - k_0^2 \mu_r \mathbf{H} \cdot \mathbf{T} \right] \, dV \\ &- \iiint_V \mathbf{T} \cdot \left[jk_0 Y_0 \mathbf{M}^{int} + \nabla \times \left(\frac{1}{\epsilon_r} \mathbf{J}^{int} \right) \right] \\ &- jk_0 Y_0 \oint_S \mathbf{T} \cdot (\mathbf{E} \times \hat{\mathbf{n}}) \, dS = 0 \end{aligned} \quad (11)$$

respectively, where $Y_0 = 1/Z_0$.

3. Finite Element Discretization

To discretize V , we subdivide it into a finite number of small volume elements such as tetrahedra, triangular prisms, or rectangular bricks. By using the edge-based vector basis functions [25], the electric field \mathbf{E} or magnetic field \mathbf{H} is expanded as

$$\mathbf{E} \text{ (or } \mathbf{H}) = \sum_{j=1}^{N_v} E_j \text{ (or } H_j) \mathbf{W}_j \quad (12)$$

where N_v denotes the total number of element edges resulting from the subdivision including those on the surface S . Also, E_j (or H_j) denote the unknown expansion coefficients equal to element edge fields and \mathbf{W}_j are the chosen vector basis functions. Note that the same basis functions are employed for both \mathbf{E} and \mathbf{H} , though this is not required.

To generate a system of equations for the fields in V , (12) is substituted into (5). Applying the Rayleigh-Ritz procedure to enforce (6) then yields

$$[A]_{N_v \times N_v} \{E\}_{N_v \times 1} + [B]_{N_v \times N_s} \{H_S\}_{N_s \times 1} = \{C\}_{N_v \times 1} \quad (13)$$

where $\{E\} = [E_1, E_2, \dots, E_{N_v}]^T$, $\{H_S\} = [H_1, H_2, \dots, H_{N_s}]^T$ with the superscript T denoting the transpose of the vector and N_s being the total number of element edges residing on the surface S . The elements of $[A]$, $[B]$ and $\{C\}$ are given by

$$A_{ij} = \iiint_V \left[\frac{1}{\mu_r} (\nabla \times \mathbf{W}_i) \bullet (\nabla \times \mathbf{W}_j) - k_0^2 \epsilon_r \mathbf{W}_i \bullet \mathbf{W}_j \right] dV \quad (14)$$

$$B_{ij} = j k_0 Z_0 \oint_S \mathbf{W}_i \bullet (\mathbf{W}_j \times \hat{\mathbf{n}}) dS \quad (15)$$

$$C_i = - \iiint_V \mathbf{W}_i \bullet \left[j k_0 Z_0 \mathbf{J}^{int} - \nabla \times \left(\frac{1}{\mu_r} \mathbf{M}^{int} \right) \right] dV. \quad (16)$$

We note that the result stated in (13) can also be obtained via a discretization of the weighted residual equation (9) provided the same expansions are used and \mathbf{T} is set to $\mathbf{T} = \mathbf{W}_i$, implying a Galerkin's formulation. Finally, a discretization of (10) or (11) yields the dual of (13) given by

$$[A']_{N_v \times N_v} \{H\}_{N_v \times 1} + [B']_{N_v \times N_s} \{E_S\}_{N_s \times 1} = \{C'\}_{N_v \times 1} . \quad (17)$$

The elements of the matrices $[A']$, $[B']$ and $\{C'\}$ are, respectively, given by the dual of (14)-(16).

4. Boundary Element Discretization

To solve the system (13) or (17), a specification of a boundary condition relating $(\mathbf{E} \times \hat{\mathbf{n}})$ and $(\mathbf{H} \times \hat{\mathbf{n}})$ is required. This is provided by the boundary integral equation (1), and to incorporate it into (13) or (17) it must first be discretized. To illustrate this let us rewrite (1) for the electric field as

$$\mathbf{E} = \mathbf{E}^{inc} + \mathbf{L}_{e1}^s (\mathbf{E} \times \hat{\mathbf{n}}) + \mathbf{L}_{e2}^s (\mathbf{H} \times \hat{\mathbf{n}}) \quad (18)$$

where \mathbf{L}_e^s was split into two parts; one (\mathbf{L}_{e1}^s) pertaining to the equivalent magnetic current and the other (\mathbf{L}_{e2}^s) to the equivalent electric current. Taking the cross product of (18) with $\hat{\mathbf{n}}$ yields

$$\mathbf{E} \times \hat{\mathbf{n}} = \mathbf{E}^{inc} \times \hat{\mathbf{n}} + \mathbf{L}_{e1}^s (\mathbf{E} \times \hat{\mathbf{n}}) \times \hat{\mathbf{n}} + \mathbf{L}_{e2}^s (\mathbf{H} \times \hat{\mathbf{n}}) \times \hat{\mathbf{n}} \quad (19)$$

which can be discretized by using (12) and applying Galerkin's procedure to find

$$[B']_{N_s \times N_s} \{E_S\}_{N_s \times 1} + [P]_{N_s \times N_s} \{E_S\}_{N_s \times 1} + [Q]_{N_s \times N_s} \{H_S\}_{N_s \times 1} = \{Y\}_{N_s \times 1} . \quad (20)$$

The matrix elements of $[B']$ are the same as those in (17) and the other matrix elements are given by

$$P_{ij} = jk_0 Y_0 \iint_S \mathbf{W}_i \bullet [\mathbf{L}_{e1}^s (\mathbf{W}_j \times \hat{\mathbf{n}}) \times \hat{\mathbf{n}}] dS \quad (21)$$

$$Q_{ij} = jk_0 Y_0 \iint_S \mathbf{W}_i \bullet [\mathbf{L}_{e2}^s (\mathbf{W}_j \times \hat{\mathbf{n}}) \times \hat{\mathbf{n}}] dS \quad (22)$$

$$Y_i = -jk_0 Y_0 \iint_S \mathbf{W}_i \bullet (\mathbf{E}^{inc} \times \hat{\mathbf{n}}) dS. \quad (23)$$

The dual of (20) can also be obtained from (1) and is given by

$$[B]_{N_s \times N_s} \{H_S\}_{N_s \times 1} + [P']_{N_s \times N_s} \{H_S\}_{N_s \times 1} + [Q']_{N_s \times N_s} \{E_S\}_{N_s \times 1} = \{Y'\}_{N_s \times 1}. \quad (24)$$

In this, the elements of $[B]$ are the same as those in (13) and the elements of $[P']$, $[Q']$ and $\{Y'\}$ are given by (21)-(23), respectively, upon replacing Y_0 with $-Z_0$, $\mathbf{L}_{e1,2}^s$ with $\mathbf{L}_{h1,2}^s$ and \mathbf{E}^{inc} with \mathbf{H}^{inc} .

5. Solution of the System

A complete system of equations for the discrete edge fields can now be obtained by combining any one of (13) and (17) with either (20) or (24). Various techniques can be employed for solving the resulting system, but it would be advantageous to use algorithms which exploit the special properties of the finite element matrices. More importantly, the subsystems (20) and (24) resulting from the discretization of the boundary integrals are fully populated and could increase the memory demand beyond $O(N)$ unless special care is exercised. In particular, to retain the $O(N)$ storage requirement, the boundary/surface S must be judiciously chosen so that the resulting boundary integral or a large portion of it is convolutional. The FFT can then be used to evaluate the integral without a need to explicitly generate and store the boundary element matrices, provided an iterative

solution such as the CG or BiCG method is employed. Below we consider specific two- and three-dimensional applications which illustrate how the boundary/surface S could be chosen to maintain the $O(N)$ storage requirement. These applications will also permit the derivation of specific forms for the matrices introduced in (13), (17), (20) and (24) as well as demonstrate the validity and effectiveness of the method. In the following we first consider a few two-dimensional applications and in this case V and V_∞ represent cross-sectional areas denoted by Ω and Ω_∞ , respectively, and S becomes a contour which will be denoted by Γ . Some three-dimensional applications are also discussed and computations are presented which are compared with reference data.

III. TWO-DIMENSIONAL ANALYSIS

For two-dimensional problems, it is sufficient to consider the transverse magnetic (TM or E -polarization) and transverse electric (TE or H -polarization) incidence separately. This reduces the problem to a scalar one and (5) or (10) becomes

$$F(\phi) = \frac{1}{2} \iint_{\Omega} \left\{ u \left[\left(\frac{\partial \phi}{\partial x} \right)^2 + \left(\frac{\partial \phi}{\partial y} \right)^2 \right] - k_0^2 v \phi^2 \right\} dx dy + \oint_{\Gamma} \phi \psi d\Gamma \quad (25)$$

where

$$\phi = E_z, \quad \psi = j k_0 Z_0 (\mathbf{H} \times \hat{\mathbf{n}}) \cdot \hat{\mathbf{z}}, \quad u = \frac{1}{\mu_r}, \quad v = \epsilon_r \quad (26)$$

for E -polarization and

$$\phi = H_z, \quad \psi = -j k_0 Y_0 (\mathbf{E} \times \hat{\mathbf{n}}) \cdot \hat{\mathbf{z}}, \quad u = \frac{1}{\epsilon_r}, \quad v = \mu_r \quad (27)$$

for H -polarization. The matrix equations (13) and (17) now reduce to

$$[A]\{\phi\} + [B]\{\psi\} = 0 \quad (28)$$

where

$$A_{ij} = \iint_{\Omega} \left[u \left(\frac{\partial N_i^g}{\partial x} \frac{\partial N_j^g}{\partial x} + \frac{\partial N_i^g}{\partial y} \frac{\partial N_j^g}{\partial y} \right) - k_0^2 v N_i^g N_j^g \right] dx dy \quad (29)$$

$$B_{ij} = \oint_{\Gamma} L_i^g L_j^g d\Gamma. \quad (30)$$

where N_i^g and L_i^g denote the chosen basis functions for the interior and boundary fields, respectively, and furthermore, N_i^g becomes the same as L_i^g at the boundary Γ . It remains to obtain the elements associated with (20) or (24). Obviously, the explicit form of these depends on the formulation of the boundary integral equation which is dependent upon the geometry of the scatterer under consideration.

1. Scattering by Grooves and Slots in a Thick Conducting Plane

Consider the geometry illustrated in Figure 2 where an infinitely long groove is cut in an infinite ground plane. For this specific configuration, Ω is the region occupied by the cross-section of the groove and Ω_{∞} is the half space above the ground plane ($y > 0$). Also, Γ consists of the straight line segment Γ_1 across the opening and the conducting boundaries forming the groove. Because of the boundary condition, the portion of the boundary integral in (25) over the conducting boundaries vanishes and, thus, we only need to consider the remaining boundary integral along Γ_1 . Below we discuss the TM and TE cases separately since they are associated with different boundary integral equations.

A. TM incidence

Using the notation defined in (26), the boundary integral equation is given by

$$\psi(x, 0) = 2\psi^{inc}(x, 0) + \frac{j}{2} \left(k_0^2 + \frac{\partial^2}{\partial x^2} \right) \int_{\Gamma_1} \phi(x') H_0^{(2)}(k_0|x-x'|) dx' \quad (31)$$

where $H_0^{(2)}(\bullet)$ denotes the zeroth order Hankel function of the second kind and a factor of two has been introduced in the right-hand side to account for the presence of the ground plane. To obtain a system corresponding to (24), (31) is discretized via Galerkin's technique, yielding

$$[B]\{\psi\} + [Q']\{\phi_b\} = \{Y'\} . \quad (32)$$

In this, $\{\phi_b\}$ denotes the portion of $\{\phi\}$ on the boundary Γ_1 , $[B]$ is the same as that in (28) and $[Q']$ and $\{Y'\}$ are given by

$$Q'_{ij} = -\frac{j}{2} \int_{\Gamma_1} L_i^g(x) \left[\left(k_0^2 + \frac{\partial^2}{\partial x^2} \right) \int_{\Gamma_1} L_j^g(x') H_0^{(2)}(k_0|x-x'|) dx' \right] dx \quad (33)$$

$$Y'_i = 2 \int_{\Gamma_1} L_i^g(x) \psi^{inc}(x, 0) dx \quad (34)$$

which can be evaluated analytically or numerically for the given L_i^g and L_j^g .

To solve for the fields $\{\phi\}$, (32) and (28) can be combined to yield

$$[A]\{\phi\} - [Q']\{\phi_b\} = -\{Y'\} \quad (35)$$

which is amenable to a unique solution and can be solved via a number of methods. However, if the CG or BiCG method is used, the FFT can be employed for the computation of $[Q']\{\phi_b\}$ without a need to generate the matrix $[Q']$. To illustrate this we refer to (33) and observe that Q'_{ij} is a function of $(i-j)$ for an equal subdivision of Γ_1 . Thus we may invoke the convolution theorem to write

$$[Q']\{\phi_b\} = \mathcal{F}^{-1} \{ \mathcal{F}\{q'\} \circ \mathcal{F}\{\phi_b\} \} \quad (36)$$

in which $q'_i = Q'_{i1}$, \mathcal{F} denotes the discrete Fourier transform and the symbol \circ implies the Hadamard product. Clearly, the use of the FFT in (36) eliminates a need to store

the entire $[Q']$ matrix (other than one row of it), thus maintaining the $O(N)$ memory requirement. We now turn to the computation of $[A]\{\phi\}$. As noted earlier, $[A]$ is an $N_v \times N_v$ square matrix resulting from the finite element discretization. Since it is assembled from the element matrices, its associated matrix product can be easily computed as

$$[A]\{\phi\} = \sum_{e=1}^{M_v} [A^e]\{\phi^e\} \quad (37)$$

where M_v is the total number of subdivision elements, $[A^e]$ is the element matrix and $\{\phi^e\}$ denotes the fields associated with the e th element. Note that $[A^e]$ are generally simple small matrices and thus the computation of (37) requires only $O(N)$ memory. The total memory demand for the solution of the system (35) is then kept to $O(N)$ since $[A]\{\phi\}$ and $[Q']\{\phi_b\}$ are the only computations in a CG or BiCG algorithm involving the use of $[A]$ and $[Q']$.

B. TE incidence

The procedure for this excitation is very similar to that outlined for the TM case. The boundary integral equation now is

$$\phi(x, 0) = 2\phi^{inc}(x, 0) + \frac{j}{2} \int_{\Gamma_1} \psi(x') H_0^{(2)}(k_0|x - x'|) dx' \quad (38)$$

where the notation defined in (27) has again been adopted. A discretization of this via Galerkin's procedure then yields

$$[B]\{\phi_b\} + [Q']\{\psi\} = \{Y'\} \quad (39)$$

where $[B]$ is the same as that in (28) and the elements of $[Q']$ and $\{Y'\}$ are now given by

$$Q'_{ij} = -\frac{j}{2} \int_{\Gamma_1} L_i^g(x) \left[\int_{\Gamma_1} L_j^g(x') H_0^{(2)}(k_0|x - x'|) dx' \right] dx \quad (40)$$

$$Y'_i = 2 \int_{\Gamma_1} L_i^g(x) \phi^{inc}(x, 0) dx. \quad (41)$$

A solution for $\{\phi\}$ and $\{\psi\}$ then follows by combining (39) with (28). As in the TM case we again observe that $[Q']\{\psi\}$ can be computed via the FFT as

$$[Q']\{\psi\} = \mathcal{F}^{-1} \{ \mathcal{F}\{q'\} \circ \mathcal{F}\{\psi\} \} \quad (42)$$

where $q'_i = Q'_{i1}$. Provided the CG or BiCG method is used, the memory requirement of the solution is only $O(N)$.

C. Numerical results

The above formulations for the TM and TE scattering by a groove and slot have been implemented using linear expansion functions. To show the capability of the method, we consider the plane wave scattering by two different structures. Figure 3 shows the backscatter radar cross section (RCS) for a rectangular groove, compared with measured data [26]. Figures 4 and 5 show: the transmission coefficient as a function of frequency and bistatic scattering patterns for a structure consisting of a wide slot having a non-uniform filling and containing a periodic array of strips in a multilayer dielectric. We note that the model employed for generating the data in Figure 4 required nearly 2500 unknowns at the high end of the spectrum. However, by using the CG or BiCG method in conjunction with the FFT, we were able to carry out the solution of the system on a workstation.

2. Scattering by Cylinders

We consider now a cylindrical scatterer of arbitrary cross-section enclosed by the

fictitious boundary Γ . The boundary integral equation then becomes

$$\phi(\boldsymbol{\rho}) = \phi^{inc}(\boldsymbol{\rho}) + \oint_{\Gamma} \left[\phi(\boldsymbol{\rho}') \frac{\partial g_0(\boldsymbol{\rho}, \boldsymbol{\rho}')}{\partial n'} + g_0(\boldsymbol{\rho}, \boldsymbol{\rho}') \psi(\boldsymbol{\rho}') \right] d\Gamma' \quad (43)$$

where $\boldsymbol{\rho}$ and $\boldsymbol{\rho}'$ denote the observation and integration points, respectively, and

$$g_0(\boldsymbol{\rho}, \boldsymbol{\rho}') = -\frac{j}{4} H_0^{(2)}(k_0 |\boldsymbol{\rho} - \boldsymbol{\rho}'|) \quad (44)$$

is the free space Green's function. A discretization of (43) via Galerkin's approach yields

$$[B]\{\phi_b\} + [P]\{\phi_b\} + [Q]\{\psi\} = \{Y\} \quad (45)$$

where $[B]$ is given by (30) and the matrix elements for $[P]$, $[Q]$ and $[Y]$ are given by

$$P_{ij} = - \oint_{\Gamma} L_i^g(\boldsymbol{\rho}) \left[\oint_{\Gamma} L_j^g(\boldsymbol{\rho}') \frac{\partial g_0(\boldsymbol{\rho}, \boldsymbol{\rho}')}{\partial n'} d\Gamma' \right] d\Gamma \quad (46)$$

$$Q_{ij} = - \oint_{\Gamma} L_i^g(\boldsymbol{\rho}) \left[\oint_{\Gamma} L_j^g(\boldsymbol{\rho}') g_0(\boldsymbol{\rho}, \boldsymbol{\rho}') d\Gamma' \right] d\Gamma \quad (47)$$

$$Y_i = \oint_{\Gamma} L_i^g(\boldsymbol{\rho}) \phi^{inc}(\boldsymbol{\rho}) d\Gamma \quad (48)$$

with $\boldsymbol{\rho}$ denoting the observation point on Γ .

The combined system of (45) and (28) now forms a complete system for the solution of $\{\phi\}$ and $\{\psi\}$. However, care must be exercised for the computation of $[P]\{\phi_b\}$ and $[Q]\{\psi\}$ to ensure an $O(N)$ memory demand for the entire system solution if the CG or BiCG method is used. In the previous examples, this was achieved by exploiting the convolutionality of the integral operators. This property is strongly dependent on the choice for Γ . It was shown that for planar Γ the boundary integral operators are convolutional, and this also holds for circular boundaries as well. Choosing Γ to be a circle tightly enclosing the cylindrical scatterer and subdividing it equally, (46) and (47)

become

$$P_{ij} = -\frac{j}{4}k_0a^2 \int_0^{2\pi} L_i^g(\varphi) \left[\int_0^{2\pi} L_j^g(\varphi') \cdot H_1^{(2)}\left(2k_0a \left| \sin \frac{\varphi - \varphi'}{2} \right| \right) \left| \sin \frac{\varphi - \varphi'}{2} \right| d\varphi' \right] d\varphi \quad (49)$$

$$Q_{ij} = \frac{j}{4}a^2 \int_0^{2\pi} L_i^g(\varphi) \left[\int_0^{2\pi} L_j^g(\varphi') H_0^{(2)}\left(2k_0a \left| \sin \frac{\varphi - \varphi'}{2} \right| \right) d\varphi' \right] d\varphi \quad (50)$$

where a denotes the radius of the circle and $H_1^{(2)}(\bullet)$ denotes the first order Hankel function of the second kind. It can be readily shown that P_{ij} and Q_{ij} are functions of $(i - j)$ and thus the matrix products associated with the boundary integrals can be efficiently evaluated via the FFT. Specifically, we have

$$[P]\{\phi_b\} = \mathcal{F}^{-1}\{\mathcal{F}\{p\} \circ \mathcal{F}\{\phi_b\}\} \quad (51)$$

$$[Q]\{\psi\} = \mathcal{F}^{-1}\{\mathcal{F}\{q\} \circ \mathcal{F}\{\psi\}\} \quad (52)$$

where $p_i = P_{i1}$ and $q_i = Q_{i1}$. In passing, we should note, though, that choosing a circular boundary enclosure may not necessarily be a memory efficient approach, particularly if the scatterer is small in one dimension. In that case, a rectangular or ogival enclosure that tightly encloses the target will most likely result in less unknowns [20]. The boundary integrals are then convolutional only when the observation and integration points are on the same side of the ogive or the rectangle, and also when they are on the parallel sides of the rectangle. Otherwise, the boundary integral has no special form and its associated matrix must therefore be stored explicitly [16].

The above formulation has been implemented and validated for a variety of geometries. Figure 6 shows the backscatter patterns for a coated ogival cylinder in comparison with the moment method data [27]. In generating the finite element - boundary integral

solution we employed a ogival enclosure in order to keep the finite element region to minimum.

IV. THREE-DIMENSIONAL ANALYSIS

The full advantage of the proposed hybrid method is realized when we consider a three-dimensional application where the memory demands are far more excessive. Therefore, having a solution method leading to an $O(N)$ memory demand is of crucial importance. In this section, we consider the problem of scattering by a cavity-backed aperture and a slot in a thick conducting plane, scattering and radiation by a microstrip patch antenna or array in a cavity, and that of scattering by a finite size object.

1. Scattering by Cavity-Backed Apertures and Slots in a Thick Conducting Plane

Consider the cavity-backed aperture illustrated in Figure 7. In this case, V_∞ is the free space region above the ground plane ($z > 0$) and V is that occupying the cavity ($-c < z < 0$). The surface S consists of the planar aperture and the conducting walls of the cavity. Because of the boundary condition the portion of the boundary integral over the conducting walls vanishes as was the case with the groove. Thus, we only need to consider the remaing portion of the integral over the aperture.

For this problem, the boundary integral equation (1) is given by

$$\mathbf{H}(\mathbf{r}) = \mathbf{H}^{inc}(\mathbf{r}) + \mathbf{H}^{ref}(\mathbf{r}) - 2jk_0Y_0 \iint_S \bar{\bar{\mathbf{G}}}_0(\mathbf{r}, \mathbf{r}') \bullet [\mathbf{E}(\mathbf{r}') \times \hat{\mathbf{z}}] dS' \quad (53)$$

where \mathbf{H}^{inc} denotes the incident field due to $(\mathbf{J}^{ext}, \mathbf{M}^{ext})$ and \mathbf{H}^{ref} is that reflected by the ground plane without the aperture. Also, $\bar{\bar{\mathbf{G}}}_0$ is the free-space dyadic Green's

function defined by

$$\bar{\bar{G}}_0(\mathbf{r}, \mathbf{r}') = \left(\bar{\bar{I}} + \frac{1}{k_0^2} \nabla \nabla \right) G_0(\mathbf{r}, \mathbf{r}') \quad (54)$$

with

$$G_0(\mathbf{r}, \mathbf{r}') = \frac{e^{-jk_0|\mathbf{r}-\mathbf{r}'|}}{4\pi|\mathbf{r}-\mathbf{r}'|}. \quad (55)$$

Multiplying (53) by $(jk_0 Z_0)$, crossing by $\hat{\mathbf{z}}$ and discretizing the resulting integral equation via Galerkin's method yields

$$[B]\{H_S\} + [Q']\{E_S\} = \{Y'\}. \quad (56)$$

In this, $[B]$ is given by (15), $[Q']$ and $\{Y'\}$ are similar to those in (24) and are more explicitly given by

$$Q'_{ij} = 2k_0^2 \iint_S [\mathbf{W}_i(\mathbf{r}) \times \hat{\mathbf{z}}] \bullet \left\{ \iint_S \bar{\bar{G}}_0(\mathbf{r}, \mathbf{r}') \bullet [\mathbf{W}_j(\mathbf{r}') \times \hat{\mathbf{z}}] dS' \right\} dS \quad (57)$$

$$Y'_i = 2jk_0 Z_0 \iint_S \mathbf{W}_i(\mathbf{r}) \bullet [\mathbf{H}^{inc}(\mathbf{r}) \times \hat{\mathbf{z}}] dS. \quad (58)$$

Obviously, the integrand singularity of Q'_{ij} is nonintegrable and it is necessary to employ the divergence theorem in order to transfer the del operators contained in $\bar{\bar{G}}_0$ to the expansion and weighting functions and this is discussed in [21]. As before, a final system of equations is obtained by combining (56) and the finite element equation (13) to give

$$[A]\{E\} - [Q']\{E_S\} = -\{Y'\}. \quad (59)$$

This can be solved using various techniques including the CG or BiCG method in conjunction with the FFT for the evaluation of the product $[Q']\{E_S\}$.

The above formulation was implemented and validated using linear basis functions for rectangular cavities and slots which are amenable to simple finite element discretizations. As an example, Figure 8 displays the backscatter RCS of a rectangular cavity and as seen, the results based on this formulation are in excellent agreement with measured data [28]. Other computations are displayed in Figures 9 and 10. In particular, Figure 9 presents the scattering by a circular cavity whereas Figure 10 displays the bistatic scattering by a material filled rectangular slot. Of course, the presented formulation is applicable to cavities filled with inhomogeneous material whereas traditional approaches are not and one such application is considered next.

2. Scattering and Radiation by Microstrip Patch Antennas in a Cavity

The structure to be considered is illustrated in Figure 11 where a microstrip patch antenna or array is residing on or embedded in a substrate which is in turn housed in a cavity recessed in a ground plane. As expected, the formulation for this problem is similar to that of scattering by a cavity-backed aperture, except in the case of radiation where the excitation is due to internal sources in the cavity. The system to be solved is therefore

$$[A]\{E\} - [Q']\{E_S\} = \{C\} \quad (60)$$

rather than (59) which is suitable for scattering computations. In (60), $\{C\}$ is given by (16) and the product $[Q']\{E_S\}$ is again evaluated via the FFT for a CG or BiCG solution.

The modeling of the conducting patches and microstrip transmission lines is carried out by setting the electric field components to zero for those element edges coinciding with

the patch. Further, an impedance load can be modeled as a post of finite conductivity joining both the patch and the base of the cavity. The antenna can be excited either by a current filament, a magnetic frill current, or a gap generator [23].

Figure 12 shows the backscatter RCS spectrum for a single patch loaded with 50 ohms at the point (x_L, y_L) . About 1280 unknowns were required for the simulation of the geometry. Notably, on the average only 100 iterations were required for the solution to converge to within 0.01 dB of the correct RCS level for each excitation with a corresponding cpu time of about 20 s on a Cray Y-MP832. The radiation patterns for a 13×16 microstrip patch array is given in Figure 13. The patches of this array are of the same size as that shown in Figure 12. They are 1.83 cm apart in the x -direction, 1.30 cm apart in the y -direction, and the cavity dimensions are 73.2 cm \times 63.7 cm \times 0.158 cm. Each patch is uniformly fed at its lower left corner and the feed was modeled by a current filament. For this example, 120935 unknowns were used and the solution converged within 100 iterations.

3. Scattering by a Finite Body

The corresponding equation to (1) for a finite body enclosed by the fictitious surface S is given by

$$\begin{aligned} \mathbf{E}(\mathbf{r}) = & \mathbf{E}^{inc}(\mathbf{r}) + \iint_S \left\{ \nabla \times \bar{\mathbf{G}}_0(\mathbf{r}, \mathbf{r}') \bullet [\mathbf{E}(\mathbf{r}') \times \hat{\mathbf{n}}'] \right. \\ & \left. - jk_0 Z_0 \bar{\mathbf{G}}_0(\mathbf{r}, \mathbf{r}') \bullet [\mathbf{H}(\mathbf{r}') \times \hat{\mathbf{n}}'] \right\} dS' \end{aligned} \quad (61)$$

for the electric field. A numerical discretization of (61) yields the matrix equation (20),

whose matrix elements can be obtained from (21)-(23). Specifically, we have

$$P_{ij} = -jk_0 Y_0 \iint_S [\mathbf{W}_i(\mathbf{r}) \times \hat{\mathbf{n}}] \bullet \left\{ \iint_S \nabla \times \bar{\bar{\mathbf{G}}}_0(\mathbf{r}, \mathbf{r}') \bullet [\mathbf{W}_i(\mathbf{r}') \times \hat{\mathbf{n}}'] dS' \right\} dS \quad (62)$$

$$Q_{ij} = -k_0^2 \iint_S [\mathbf{W}_i(\mathbf{r}) \times \hat{\mathbf{n}}] \bullet \left\{ \iint_S \bar{\bar{\mathbf{G}}}_0(\mathbf{r}, \mathbf{r}') \bullet [\mathbf{W}_i(\mathbf{r}') \times \hat{\mathbf{n}}'] dS' \right\} dS \quad (63)$$

The implementation of the above formulation for an arbitrary body has not yet been carried out. A major difficulty is the large number of unknowns on S even for small bodies. To overcome this, a cylindrical enclosure may be chosen so that the integrals over the cylindrical surface become two-dimensional convolutions and can, thus, be evaluated via the FFT, provided the CG or BiCG method is employed for the solution of the system. This idea has been tested for a body of revolution [24] and Figure 14 displays the bistatic scattering patterns for an ogive as obtained by this method and the moment method [29].

V. CONCLUSION

In this paper we reviewed a hybrid finite element – boundary integral method for scattering and radiation applications. The method involves the introduction of a fictitious boundary enclosing the scatterer which serves to decouple the fields in the regions interior and exterior to the boundary. The fields in the interior region are formulated via the finite element method whereas those in the exterior region are represented by the boundary integrals involving the free space Green's function. The interior and exterior fields are then coupled by invoking the continuity of the tangential boundary fields, resulting in a complete system for the solution of the fields internal to and on the fictitious boundary.

Of particular interest in the proposed hybrid formulation is the choice of the fictitious

boundary so that the resulting boundary integrals are convolutional. If so, they can then be evaluated via the FFT when an iterative solution of the system such as the conjugate gradient or biconjugate gradient method is employed. This avoids a need to generate the matrix and since the finite element discretization results in sparse and banded matrices, the entire system solution requires a low $O(N)$ storage. The proposed technique, therefore, holds a promise for treating large structures without a compromise in accuracy. We should note, however, that this technique, like others involving the use of boundary integral equations over closed surfaces or contours, may be associated with fictitious internal resonance phenomena which can be eliminated by combining the E and H field boundary integral equations. Such difficulties do not, of course, arise when the boundaries are not closed such as in the case of aperture problems.

Finally, we note that in all cases considered in this paper the final system of equations is symmetric, due to the employment of Galerkin's method for the discretization of the boundary integral equations. As a result, the BiCG method is more favorable than the CG method since it requires only one matrix-vector product computation in each iteration and also since it converges faster.

REFERENCES

- [1] K. K. Mei and J. Van Bladel, "Scattering by perfectly conducting rectangular cylinder," *IEEE Trans. Antennas Propagat.*, vol. AP-11, pp. 185-192, March 1963.
- [2] T. K. Wu and L. L. Tsai, "Scattering by arbitrarily cross sectioned layered lossy dielectric cylinders," *IEEE Trans. Antennas Propagat.*, vol. AP-25, pp. 518-524, July 1977.

- [3] S. M. Rao, D. R. Wilton, and A. W. Glisson, "Electromagnetic scattering by surfaces of arbitrary shape," *IEEE Trans. Antennas Propagat.*, vol. AP-30, pp. 409-418, May 1982.
- [4] K. Umashankar, A. Taflove, and S. M. Rao, "Electromagnetic scattering by arbitrary shaped three dimensional homogeneous lossy dielectric objects," *IEEE Trans. Antennas Propagat.*, vol. AP-34, pp. 758-766, June 1986.
- [5] J. H. Richmond, "Scattering by a dielectric cylinder of arbitrary cross-section shape," *IEEE Trans. Antennas Propagat.*, vol. AP-13, pp. 334-341, March 1965.
- [6] J. H. Richmond, "TE-wave scattering by a dielectric cylinder of arbitrary cross-section shape," *IEEE Trans. Antennas Propagat.*, vol. AP-14, pp. 460-464, July 1966.
- [7] D. E. Livesay and K. M. Chen, "Electromagnetic fields induced inside arbitrarily shaped biological bodies," *IEEE Trans. Microwave Theory Tech.*, vol. MTT-22, pp. 1273-1280, Dec. 1974.
- [8] D. H. Schaubert, D. R. Wilton, and A. W. Glisson, "A tetrahedral modelling method for electromagnetic scattering by arbitrarily shaped inhomogeneous dielectric bodies," *IEEE Trans. Antennas Propagat.*, vol. AP-32, pp. 77-85, Jan. 1984.
- [9] J. L. Mason, "Finite element solution for electromagnetic scattering from two-dimensional bodies," Ph.D. dissertation, The University of Michigan, Ann Arbor, 1982.
- [10] R. Mittra and O. Ramahi, "Absorbing boundary conditions for the direct solution of partial differential equations arising in electromagnetic scattering problems," in

PIER 2: Finite Element and Finite Difference Methods in Electromagnetic Scattering, M. A. Morgan, Ed. New York: Elsevier, 1990, ch. 4.

- [11] A. F. Peterson and S. P. Castillo, "A frequency-domain differential equation formulation for electromagnetic scattering from inhomogeneous cylinders," *IEEE Trans. Antennas Propagat.*, vol. AP-37, pp. 601-607, May 1989.
- [12] S. K. Chang and K. K. Mei, "Application of the unimoment method to electromagnetic scattering of dielectric cylinders," *IEEE Trans. Antennas Propagat.*, vol. AP-24, pp. 35-42, Jan. 1976.
- [13] M. A. Morgan and K. K. Mei, "Finite-element computation of scattering by inhomogeneous penetrable bodies of revolution," *IEEE Trans. Antennas Propagat.*, vol. AP-27, pp. 202-214, March 1979.
- [14] S. K. Jeng and C. H. Chen, "On variational electromagnetics: theory and application," *IEEE Trans. Antennas Propagat.*, vol. AP-32, pp. 902-907, Sept. 1984.
- [15] S. P. Marin, "Computing scattering amplitudes for arbitrary cylinders under incident plane waves," *IEEE Trans. Antennas Propagat.*, vol. AP-30, pp. 1045-1049, Nov. 1982.
- [16] J. M. Jin and V. V. Liepa, "Application of hybrid finite element method to electromagnetic scattering from coated cylinders," *IEEE Trans. Antennas Propagat.*, vol. AP-36, pp. 50-54, Jan. 1988.
- [17] Z. Gong and A. W. Glisson, "A hybrid equation approach for the solution of electromagnetic scattering problems involving two-dimensional inhomogeneous dielectric

- cylinders," *IEEE Trans. Antennas Propagat.*, vol. AP-38, pp. 60-68, Jan. 1990.
- [18] J. M. Jin and J. L. Volakis, "TE scattering by an inhomogeneously filled aperture in a thick conducting plane," *IEEE Trans. Antennas Propagat.*, vol. 38, pp. 1280-1286, Aug. 1990.
- [19] J. M. Jin and J. L. Volakis, "TM scattering by an inhomogeneously filled aperture in a thick conducting plane," *Proc. Inst. Elec. Eng., part H*, vol. 137, pp. 153-159, June 1990.
- [20] J. D. Collins, J. M. Jin, and J. L. Volakis, "A combined finite element – boundary element formulation for solution of two-dimensional problems via CGFFT", *Electromagnetics*, vol. 10, no. 4, pp. 423-437, 1990.
- [21] J. M. Jin and J. L. Volakis, "A finite element – boundary integral formulation for scattering by three-dimensional cavity-backed apertures," *IEEE Trans. Antennas Propagat.*, vol. AP-39, pp. 97-104, Jan. 1991.
- [22] J. M. Jin and J. L. Volakis, "Electromagnetic scattering by and transmission through a three-dimensional slot in a thick conducting plane," *IEEE Trans. Antennas Propagat.*, vol. AP-39, April 1991.
- [23] J. M. Jin and J. L. Volakis, "Scattering and radiation from microstrip patch antennas and arrays residing in a cavity," *IEEE Trans. Antennas Propagat.*, submitted for publication.
- [24] J. D. Collins and J. L. Volakis, "A combined finite element – boundary element formulation for solution of axially symmetric bodies," Radiation Laboratory Technical

Report 025921-18-T, The University of Michigan, Jan. 1991.

- [25] M. L. Barton and Z. J. Cendes, "New vector finite elements for three-dimensional magnetic field computation," *J. Appl. Phys.*, vol. 61, pp. 3919-3921, April 1987.
- [26] W. J. Kent, personal communication.
- [27] J. M. Jin and V. V. Liepa, "Simple moment method program for computing scattering from complex cylindrical obstacles," *Proc. Inst. Elec. Eng., part H*, vol. 136, no. 4, pp. 321-329, Aug. 1989.
- [28] A. K. Dominek, H. T. Shamansky, and N. Wang, "Scattering from three-dimensional cracks," *IEEE Trans. Antennas Propagat.*, vol. AP-37, pp. 586-591, May 1989.
- [29] J. M. Putnam and L. N. Medgyesi-Mitschang, "Combined field integral equation formulation for axially inhomogeneous bodies of revolution," McDonnell Douglas Research Laboratories Report QA003, Dec. 1987.

FIGURE CAPTIONS

Fig. 1 Geometry of the scattering/radiation problem.

Fig. 2 Geometry of a two-dimensional groove.

Fig. 3 Backscatter RCS for a 2.5 cm wide and 1.25 cm deep rectangular groove as a function of frequency. H -polarization, $\varphi^{inc} = 10^\circ$.

Fig. 4 Transmission coefficient as a function of frequency for a truncated strip grating at normal incidence. Top and bottom layers: $\epsilon_r = 2.56$, $\mu_r = 1.0$, 0.2 cm thick; middle layer: $\epsilon_r = 4.0$, $\mu_r = 1.0$, 0.2 cm thick.

Fig. 5 Bistatic scattering patterns for the geometry in Figure 4 at 10 GHz and $\varphi^{inc} = 60^\circ$. (a) E -polarization; (b) H -polarization.

Fig. 6 Backscatter pattern for a $4\lambda \times 1\lambda$ perfectly conducting ogival cylinder with a 0.05λ thick material coating having $\epsilon_r = 3 - j5$, $\mu_r = 1.5 - j0.5$. (a) E -polarization; (b) H -polarization.

Fig. 7 Geometry of a cavity-backed aperture in a ground plane.

Fig. 8 Backscatter pattern for a 16 inch long, 0.1968 inch wide and 0.837 inch deep cavity at $f = 12$ GHz. $\mathbf{E}^{inc} = \hat{y}E$, $\varphi^{inc} = 0$.

Fig. 9 Backscatter pattern for an 1 inch deep circular cavity having a diameter of 1 inch at $f = 16$ GHz.

Fig. 10 Bistatic scattering pattern at normal incidence for a 1.2λ long, 0.25λ wide and 0.25λ deep slot filled with the material of $\epsilon_r = 2 - j$ and $\mu_r = 1.2 - j0.1$. $\mathbf{E}^{inc} = \hat{\mathbf{x}}E$ and circles correspond to the scaled two-dimensional solution [19].

Fig. 11 Geometry of a microstrip patch array in a cavity.

Fig. 12 Backscatter RCS versus frequency for a single patch loaded with 50 ohms. The cavity is 0.158 cm deep and filled with a substrate having $\epsilon_r = 2.17$ and a loss tangent of 0.001. $\theta^{inc} = 60^\circ$, $\varphi^{inc} = 45^\circ$, $\mathbf{E}^{inc} = \hat{\theta}E$.

Fig. 13 Radiation pattern of the 13×16 microstrip patch array equally fed at the lower left corner of each patch. (—) $\varphi = 0 - \pi$ plane; (- - -) $\varphi = \pi/2 - 3\pi/2$ plane. (a) $f = 2.62$ GHz. (b) $f = 3.55$ GHz.

Fig. 14 Bistatic scattering pattern for a 1.0λ long conducting ogive having a diameter of 0.176λ at its center.

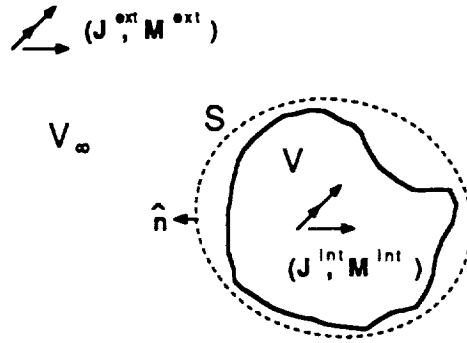


Fig. 1

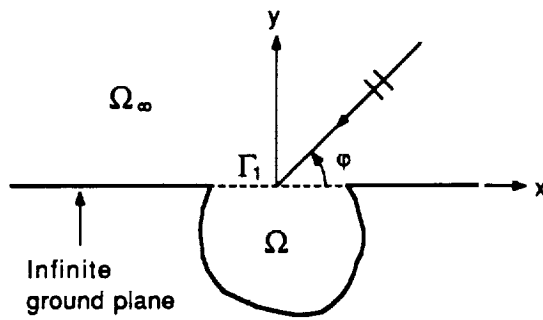


Fig. 2

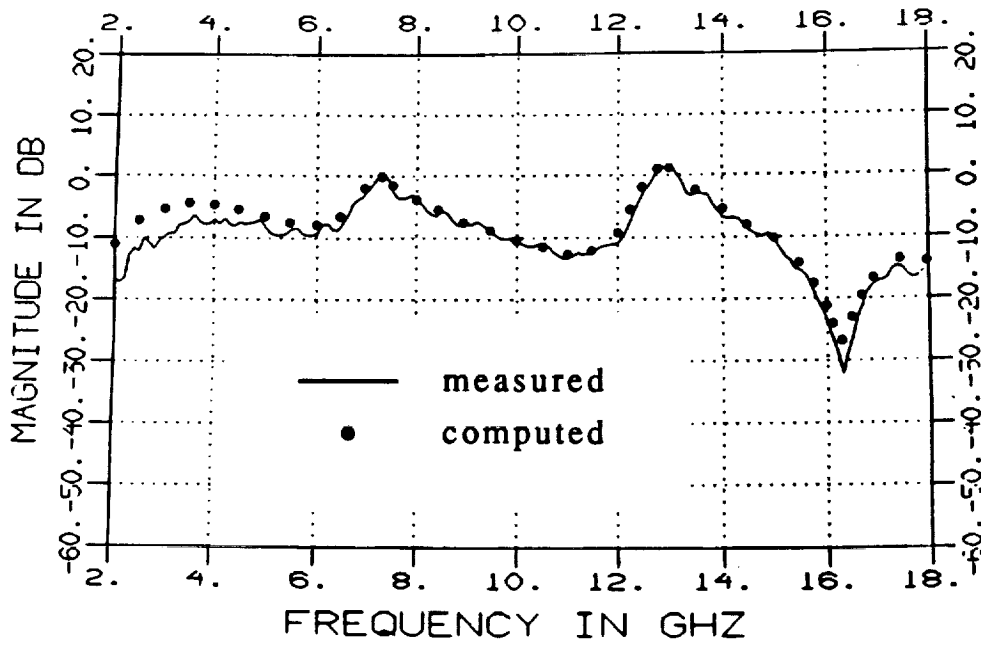


Fig. 3

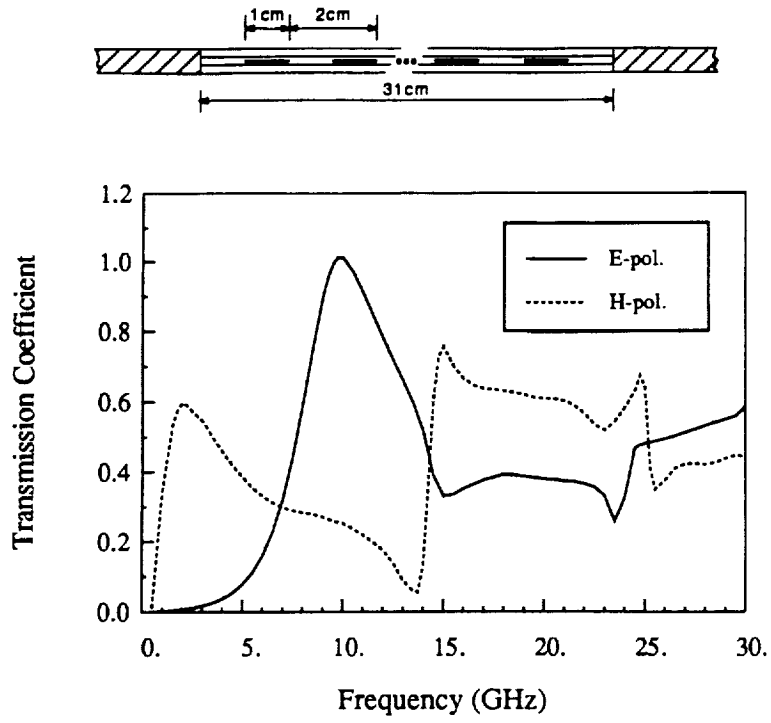


Figure 4

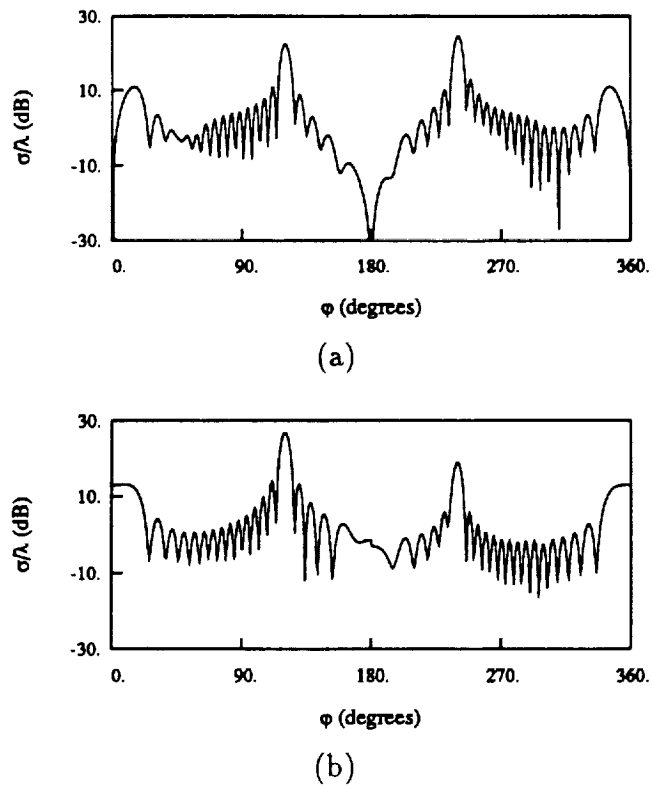
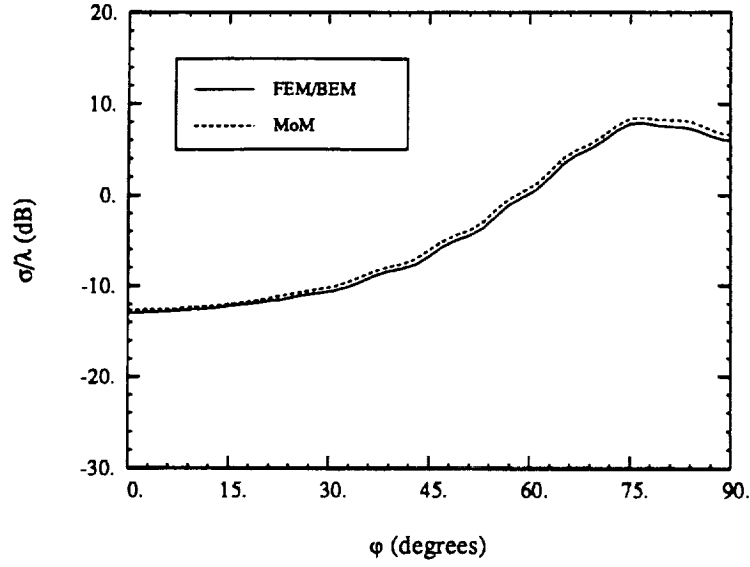
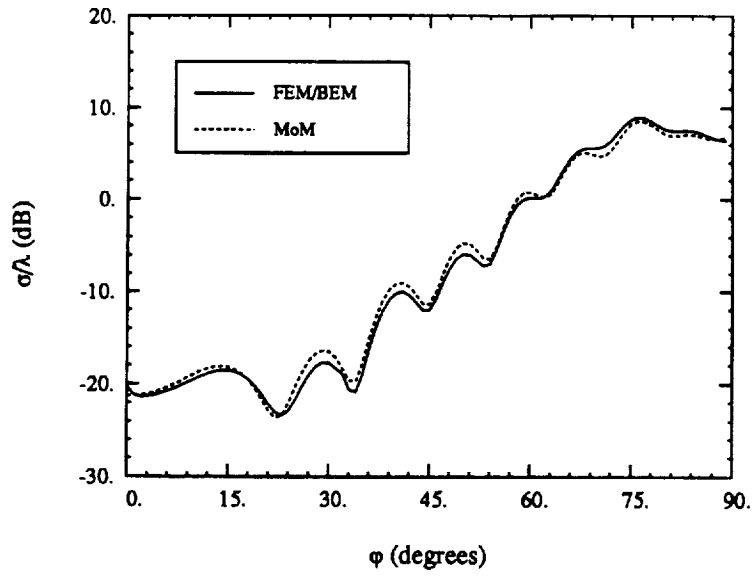


Figure 5



(a)



(b)

Figure 6

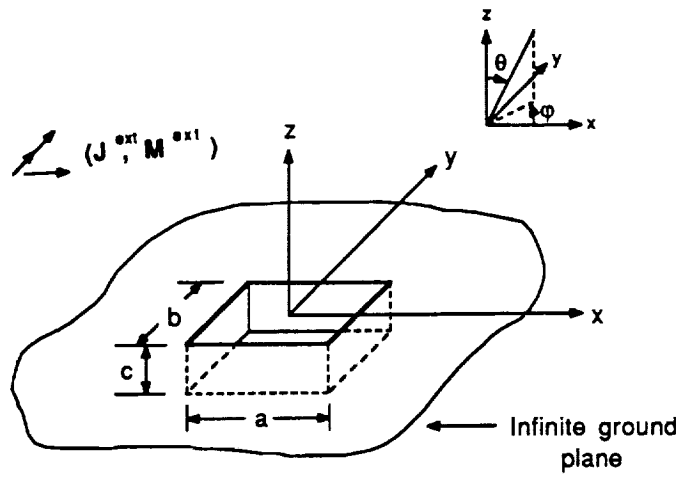


Fig. 7

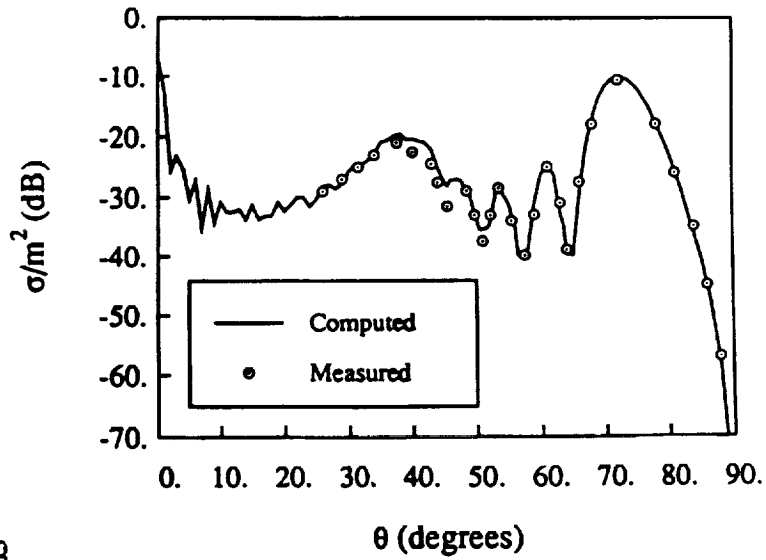
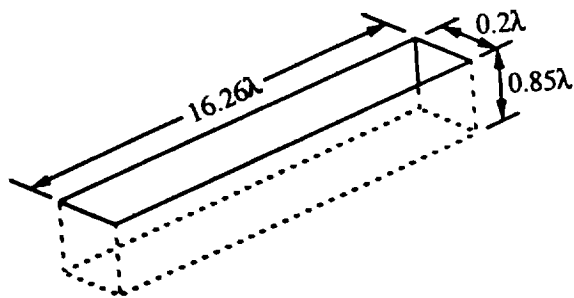


Fig. 8

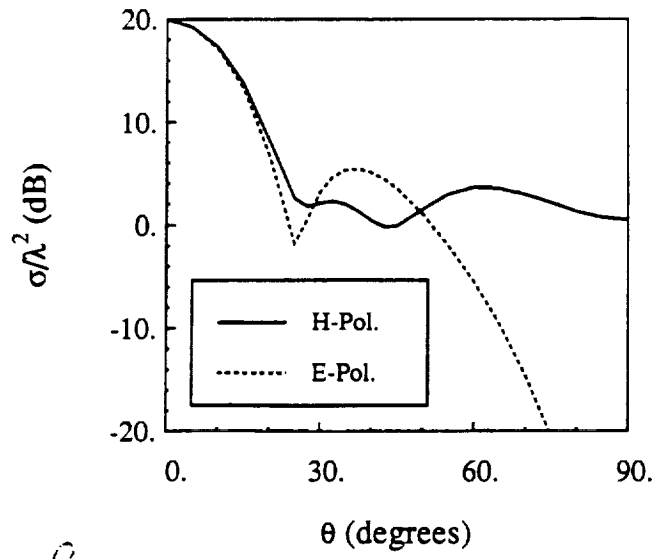


Fig. 9

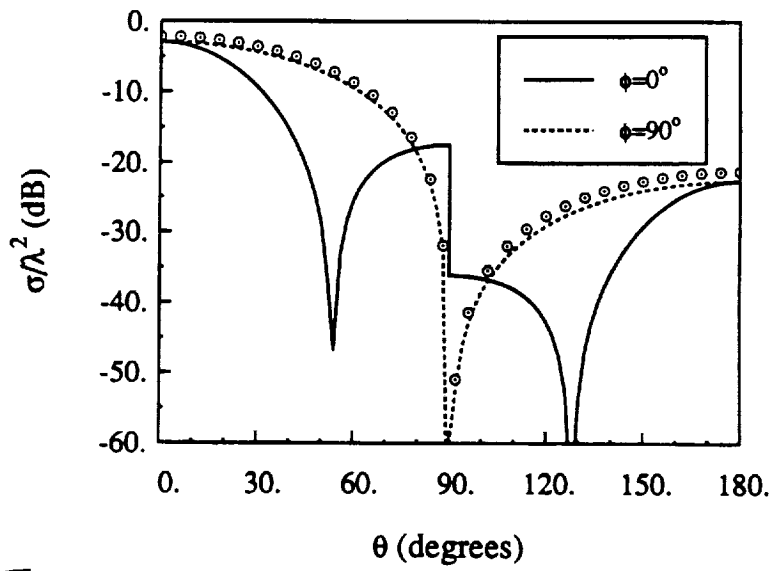


Fig. 10

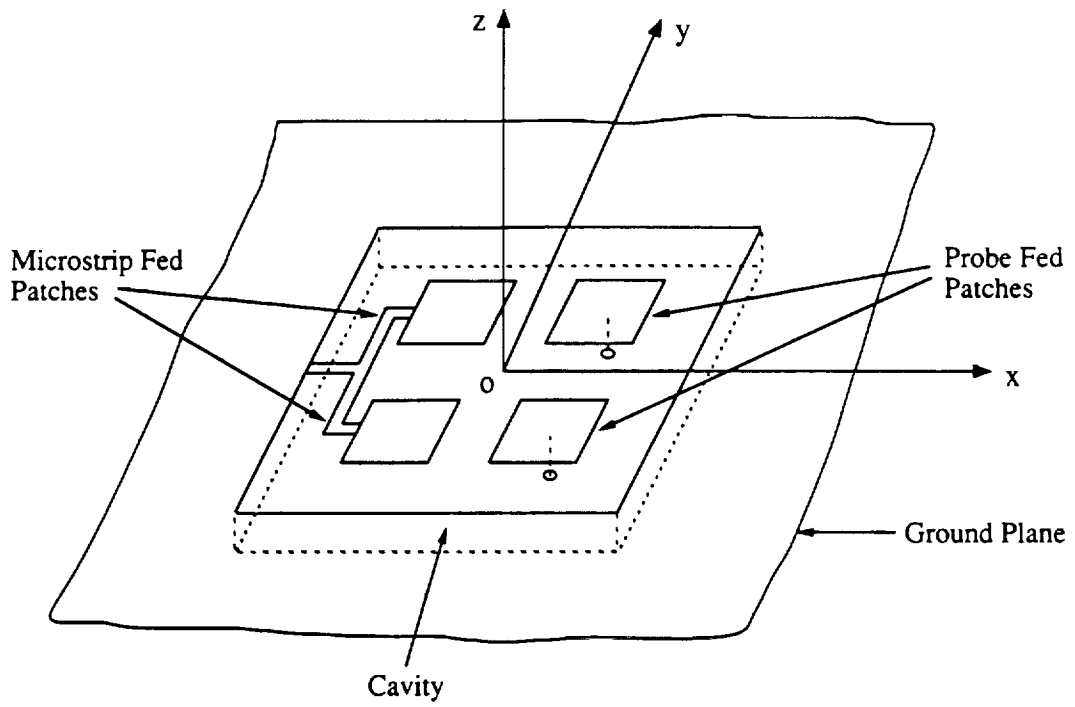


Fig. 11

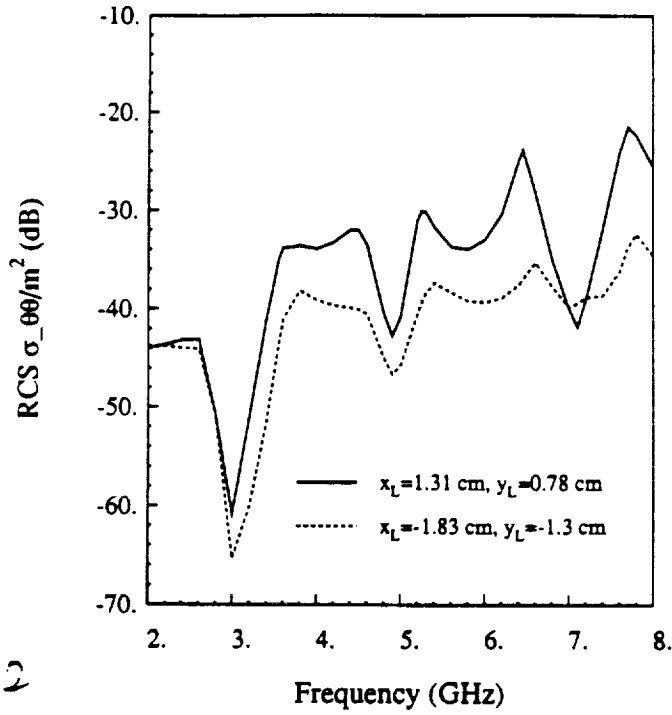
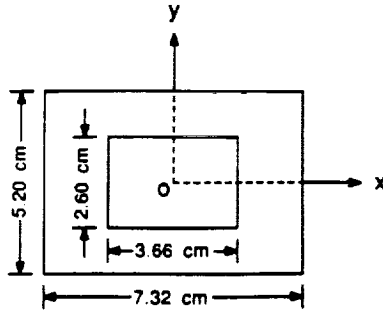


Fig. 12

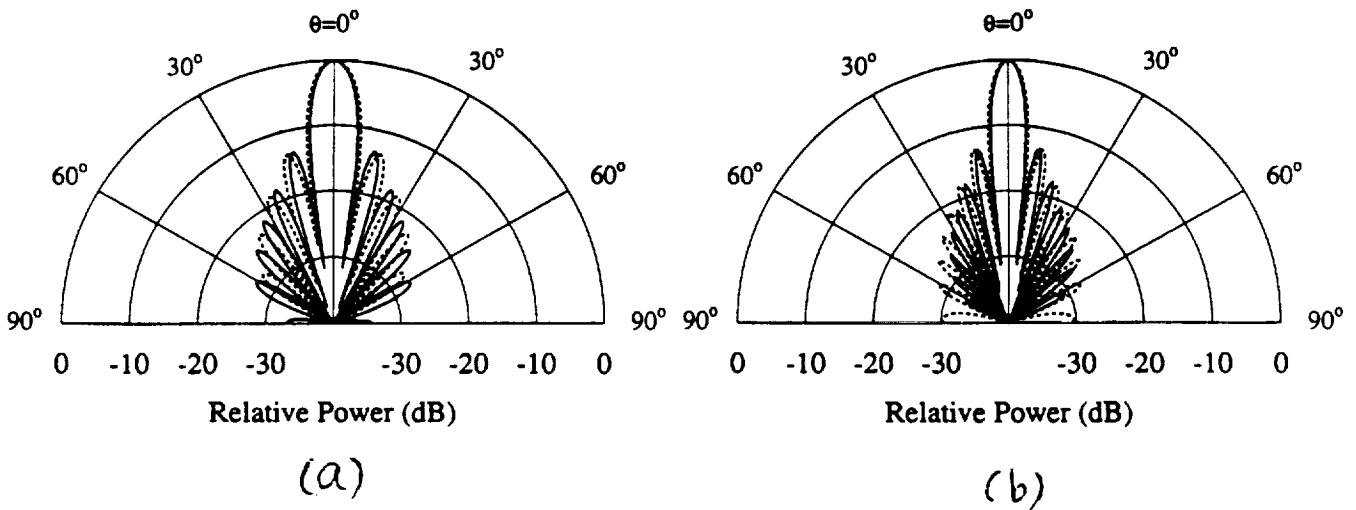


Fig. 13

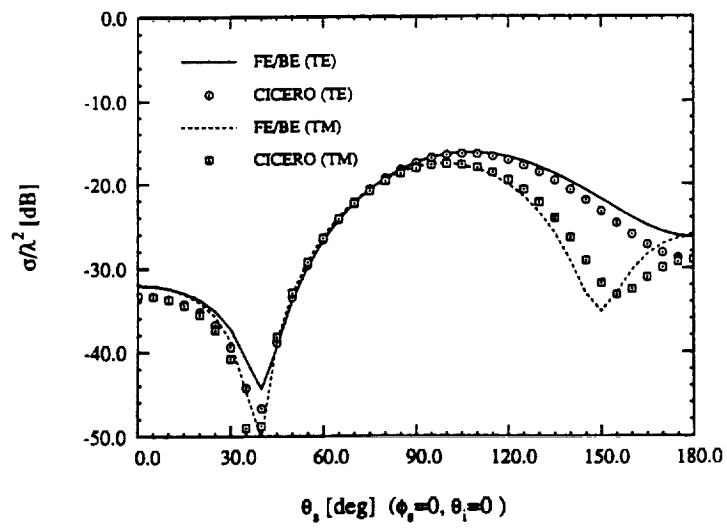
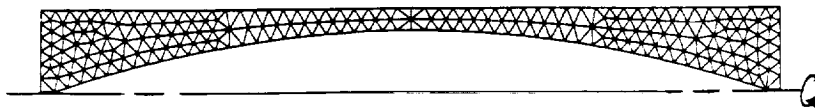


Fig. 14